The epitranscriptome m^{6}A writer METTL3 promotes chemo- and radioresistance in pancreatic cancer cells

KOSUKE TAKETO[1-3*], MASAMITSU KONNO[2,3*], AYUMU ASAI[2,3], JUN KOSEKI[2], MASAYASU TORATANI[1,2], TAROH SATOH[3], YUICHIRO DOKI[4], MASAKI MORI[4], HIDESHI ISHII[2,3] and KAZUHIKO OGAWA[1]

Departments of [1]Radiation Oncology, [2]Medical Data Science, [3]Cancer Frontier Science, and [4]Gastroenterological Surgery, Osaka University Graduate School of Medicine, Osaka 565-0871, Japan

Received September 13, 2017; Accepted October 16, 2017

DOI: 10.3892/ijo.2017.4219

Abstract. N^6-methyladenosine (m^{6}A) is the most abundant epitranscriptome modification in mammalian mRNA. Recent years have seen substantial progress in m^{6}A epitranscriptomics, indicating its crucial roles in the initiation and progression of cancer through regulation of RNA stabilities, mRNA splicing, microRNA processing and mRNA translation. However, by what means m^{6}A is dynamically regulated or written by enzymatic components represented by methyltransferase-like 3 (METTL3) and how m^{6}A is significant for each of the numerous genes remain unclear. We focused on METTL3 in pancreatic cancer, the prognosis of which is not satisfactory despite the development of multidisciplinary therapies. We established METTL3-knockdown pancreatic cancer cell line using short hairpin RNA. Although morphologic and proliferative changes were unaffected, METTL3-depleted cells showed higher sensitivity to anticancer reagents such as gemcitabine, 5-fluorouracil, cisplatin and irradiation. Our data suggest that METTL3 is a potent target for enhancing therapeutic efficacy in patients with pancreatic cancer. In addition, we performed cDNA expression analysis followed by Gene Ontology and protein-protein interaction analysis using the Database for Annotation, Visualization, and Integrated Discovery and Search Tool for the Retrieval of Interacting Genes/Proteins databases, respectively. The results demonstrate that METTL3 was associated with mitogen-activated protein kinase cascades, ubiquitin-dependent process and RNA splicing and regulation of cellular process, suggesting functional roles and targets of METTL3.

Correspondence to: Professor Hideshi Ishii, Department of Medical Data Science, Osaka University Graduate School of Medicine, Suita, Yamadaoka 2-2, Osaka 565-0871, Japan
E-mail: hishii@gesurg.med.osaka-u.ac.jp

Professor Kazuhiko Ogawa, Department of Radiation Oncology, Osaka University Graduate School of Medicine, Suita, Yamadaoka 2-2, Osaka 565-0871, Japan
E-mail: kogawa@radonc.med.osaka-u.ac.jp

*Contributed equally

Key words: RNA methylation, METTL3, chemosensitivity, radiosensitivity

Introduction

It has been >70 years since Waddington first proposed the notion of 'epigenetics' (1), in which he defined it as 'the relation between phenotypes and genotypes'. Although the full scope of epigenetics is yet to be determined, its general meaning refers to chemical modifications such as DNA methylation, histone acetylation/methylation, protein glycosylation, and RNA methylation that alter gene expression without changing nucleotide sequences. To date, >100 RNA chemical modifications have been discovered (2). Among them, N^6-methyladenosine (m^{6}A) is the most abundant modification on epitranscriptome in mRNAs, which is introduced by the human methyltransferase complex composed of methyltransferase-like 3 (METTL3), METTL14 and Wilms tumor 1-associated protein (WTAP) complex (3,4). While m^{6}A was identified in the 1970s (5,6), even the precise distribution was seldom elucidated until recently. With the advent of anti-m^{6}A antibody and methylated RNA immunoprecipitation sequencing (MeRIP-Seq) technology, there has been significant progress in the field of m^{6}A in recent years. M^{6}A site mapping reveals that m^{6}A peaks are typically located in the vicinity of the stop codon as well as 5'-untranslated regions (UTRs) and m^{6}A tends to be found in the RR-A-CH (R = A/G, H = A, C, or U) consensus motif (7-11). Previous studies reported that m^{6}A RNA methylation is a dynamic reversible phenomenon (12,13) in which the METTL3-METTL14-WTAP complex works as m^{6}A writers; fat mass- and obesity-associated protein (FTO) and AlkB homolog 5 (ALKBH5) demethylate as m^{6}A erasers (12,13); and YTH domain family and heterogeneous nuclear ribonucleoprotein C (HNRNPC) and its family proteins recognize m^{6}A as m^{6}A readers (7,14). However, comprehensive understanding of this dynamic regulatory system remains elusive. The presence of m^{6}A seems to affect mRNA fate and function in various ways such as circadian clock (15), mRNA degradation (16,17), translational alteration (10,18,19), splicing effects (3,7,14,20), microRNA maturation (21,22), cell reprogramming (11,23,24), long non-coding RNA (lncRNA) inactivation, X-inactive

specific transcript (XIST) (25), and RNA-mediated response to ultraviolet (UV)-induced DNA damage (26). Using previously reported MeRIP-Seq data, computational *in silico* analysis has built an m^6A-driven network of m^6A-driven genes, suggesting various roles of m^6A (27).

Despite increased understanding about m^6A, direct or indirect target genes of METTL3 or m^6A remain unclear. Additionally, the precise role of METTL3 in cancer cells is unknown. To evaluate the aforementioned issues, we focused on the role of METTL3 in pancreatic cancer cells in patients whose prognosis remains poor despite the recent development of multidisciplinary therapies. We investigated the role of METTL3 *in vitro* using human pancreatic cancer lines and demonstrated the functional changes in METTL3 knockdown (KD) cells.

Materials and methods

Cell lines and culture conditions. Human pancreatic adenocarcinoma cell lines, MIA PaCa-2, were purchased from the the American Type Culture Collection (ATCC; Manassas, VA, USA. The cells were maintained in Dulbecco's modified Eagle's medium (DMEM) low glucose (Nacalai Tesque, Inc., Kyoto, Japan) supplemented with 10% fetal bovine serum (FBS; Thermo Fisher Scientific, Waltham, MA, USA) and 1% penicillin/streptomycin (Life Technologies, Carlsbad, CA, USA) in 5% CO_2 at 37˚C.

Knockdown by short hairpin RNA transfection. For lentiviral particle production, 293FT cells were seeded 24 h before lentiviral infection and cotransfected with pCMV-VSV-G-RSV-Rev and pCAG-HIVgp (provided by Dr Miyoshi from the RIKEN BioResource, Tokyo, Japan) plasmid using Lipofectamine 3000 and P3000 Reagent (Thermo Fisher Scientific) as described in the standard protocol of Lipofectamine 3000. Target sequences of METTL3 short hairpin RNA (shRNA) were 5'-CCAGTCATAAACCAGATGAAA-3'. The collected viral soup was centrifuged at 12,000 x g for 5 min, and the supernatant was filtered with 0.22-μm pores (Merck Millipore, Billerica, MA, USA). Purified viral particles were infected to target MIA PaCa-2 cells with polybrene (Sigma-Aldrich, St. Louis, MO, USA). After a 24-h incubation, infected cells were selected with 2 μg/ml of puromycin (InvivoGen, Inc., San Diego, CA, USA) for 5 days.

RNA extraction and quantitative reverse transcriptase polymerase chain reaction (qRT-PCR). Total RNA was extracted from cultured cells using TRIzol reagent (Thermo Fisher Scientific) and cDNA was synthesized with ReverTra Ace (Toyobo Co., Ltd., Osaka, Japan). Quantitative RT-PCR was performed with Thunderbird SYBR qPCR Mix (Toyobo) using LightCycler 2.0 (Roche Molecular Systems, Inc., Pleasanton, CA, USA). Furthermore, data were analyzed by the $\Delta\Delta$Ct method, in which target genes were normalized to glyceraldehyde-3-phosphate dehydrogenase (GAPDH). The following primers were used in the present study: GAPDH-F, 5'-GCCCAATACGACCAAATCC-3' and GAPDH-R, 5'-AGCCACATCGCTCAGACAC-3'; METLL3-F, 5'-CGTACTACAGGATGATGGCTTTC-3' and METTL3-R, 5'-TTTCATCTACCCGTTCATACCC-3'.

Western blot analysis. Plated cells were carefully washed twice with phosphate-buffered saline (PBS; Thermo Fisher Scientific). Next, total protein was extracted with radioimmunoprecipitation assay buffer (Pierce, Rockford, IL, USA) supplemented with 1% of Halt Protease Inhibitor Cocktail (100X) and Halt Phosphatase Inhibitor Cocktail (100X; Thermo Fisher Scientific). Isolated proteins were electrophoresed on 4-20% Mini-PROTEAN TGX Precast protein gels (Bio-Rad Laboratories, Hercules, CA, USA) and transferred to Blot 2 PVDF Mini Stack membranes (Thermo Fisher Scientific) using iBlot 2 Dry Blotting System (Life Technologies). The membrane was blocked with 5% skim milk (Wako Pure Chemical Industries, Ltd., Osaka, Japan) for 1 h at room temperature and reacted with appropriate dilutions of primary antibody overnight at 4˚C. The membrane was washed with Tris-buffered saline-Tween (TBST) 6 times for 5 min each, followed by incubation with HRP-linked, anti-rabbit immunoglobulin G (GE Healthcare Biosciences, Little Chalfont, UK) for 1 h at room temperature. The membrane was washed again with TBST 6 times for 5 min each. Next, the secondary antibodies were identified using detection reagent Clarity Western ECL substrate (Bio-Rad Laboratories). Images were acquired with ImageQuant LAS 4000 (GE Healthcare Biosciences). The following primary antibodies were used in this study: METTL3 (Proteintech Group Inc., Chicago, IL, USA; rabbit, #15073-1-AP, 1:1,000) and β-actin (Cell Signaling Technology, Danvers, MA, USA; rabbit, #4967, 1:10,000).

Proliferation assay. Cells were seeded in 96-well plates with 1,500 cells/well containing 100 μl of DMEM. After incubation for 48, 72 and 96 h, 10 μl of 25% glutaraldehyde (Wako Pure Chemical Industries) was added to fixed cells, stained with 100 μl of 0.05% crystal violet (Sigma-Aldrich) with 20% methanol, solubilized the stain in 150 μl of 50% ethanol supplemented with 0.05 M NaH_2PO_4, and light absorbance of the solution was measured at 595 nm on the EnSpire microplate reader (Perkin-Elmer, Inc., Waltham, MA, USA).

Sphere formation assay. We performed sphere formation assay using the limiting dilution method. Cultured cells were collected in serum-free DMEM/F-12 with GlutaMAX, bFGF, EGF, B-27 and N_2 supplements (Thermo Fisher Scientific). Cell numbers were diluted to 10 cells/ml, then 100-μl aliquots were dispensed into each well in 96-Well Clear Round Bottom Ultra Low Attachment Microplate (Costar culture plate; Corning Costar, Corning, NY, USA). Sphere diameters were measured after 15 days of incubation.

Chemosensitivity assay. Cells were plated in 96-well plates at a density of 900 cells/90 μl/well. After incubating for 24 h, 10 μl of fluorouracil (5-FU), cisplatin (CDDP), gemcitabine (GEM) and PBS control were added. The final concentrations were 5-FU at 0, 10, 20, 40, 60, 80, 100 and 120 μM; CDDP at 0, 0.625, 1.25, 2.5, 5, 10, 20 and 50 μM; and GEM at 0, 8, 16, 32, 64 and 128 nM. After 3 to 5 days of incubation, crystal violet staining was performed and absorbance at 595 nm was measured.

Radiosensitivity assay. Radiosensitivity assay was performed as previously described (28). Cells were plated into 6-cm

dishes (N=4) at concentrations of 50, 100, 200, 400, 1,000, and 2,500 cells/dish and irradiated with 0, 2, 4, 6, 8 and 10 Gy, respectively, using Gammacell 40 Exactor (Nordion, Inc., Ottawa, ON, Canada) and incubated for 10 days. Cells were fixed with 25% glutaraldehyde and stained with crystal violet. Colonies with >50 cells were counted under the microscope.

Chemoradiosensitivity assay. Cells were seeded into four 96-well plates, respectively, in the same way as the chemosensitivity assay. In 2 of 4 plates, 10 μl of drug was added to a final concentration of 20 μM of CDDP or 16 nM of GEM after 24-h incubation. Just after drug administration, a 4-Gy dose was irradiated using the Gammacell 40 Exactor. After 5 days of incubation, all plates were fixed and stained with crystal violet and absorbance at 595 nm was measured.

Annexin V assays. GEM was added (final concentration 16 nM) after $4x10^4$ cells were seeded in 10-cm dishes and incubated for 24 h. PBS was used as a control. After incubation for 48 h, apoptosis assay was performed using the Annexin V-FITC apoptosis detection kit (Nacalai Tesque) in accordance with the instructional protocols. Fluorescence intensity of Annexin V-FITC and PI were measured after gating viable cells on FSC vs. SSC dot plots using the BD FACSCanto II system (BD Biosciences, Franklin Lakes, NJ, USA).

Human apoptosis proteome profiler array. The relative expression levels of 35 human apoptosis-related proteins were detected using the Proteome Profiler Array Human Apoptosis Array kit (R&D Systems, Minneapolis, MN, USA). Cells on a 10-cm dish were rinsed with PBS 3 times and solubilized with lysis buffer supplemented with 1% of Halt Protease Inhibitor Cocktail (Thermo Fisher Scientific). Experiments were performed in accordance with the manufacturer's instructions.

cDNA expression study. TRIzol reagents were used to extract total RNA from cultured cells, and RNA quality was checked (RNA concentration >0.5 μg/μl and OD260/280, 1.8-2.0). These samples were outsourced for DNA microarray analysis using 3D-Gene (Toray Industries, Inc., Tokyo, Japan).

Data set comparison and Gene Ontology enrichment analysis. Differentially expressed genes whose fold changes were >2 or <1/2 in METTL3 KD cells underwent Gene Ontology (GO) functional enrichment analysis using the Database for Annotation, Visualization and Integrated Discovery (DAVID) v6.8 (29).

Protein-protein interaction network construction. The functional interactions among differentially expressed genes were conducted with the online Search Tool for the Retrieval of Interacting Genes/Proteins (STRING, available at https://string-db.org/) database (confidence score ≥0.700) (30). Network edges were visualized using a popular open source software Cytoscape version 3.5.1 (available at http://www.cytoscape.org/) (31); subsequently, modules (highly interconnected regions) in a network were identified using the Cytoscape plug-in MCODE (32), version 1.4.2 (available at http://apps.cytoscape.org/apps/mcode), with parameters of degree cut-off = 2, node score cut-off = 2, k-core = 2, and max depth = 100. Next, genes in each module were analyzed with DAVID to identify rich GO terms.

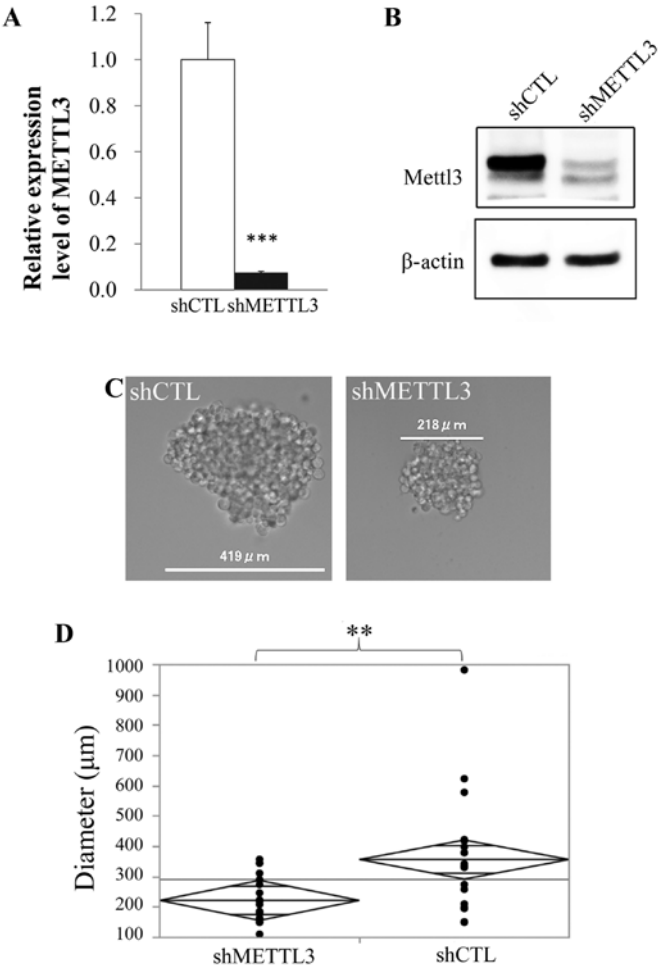

Figure 1.Knockdown (KD) of METTL3 by short hairpin RNA. (A) qRT-PCR (n=3) and (B) western blot analysis of METTL3 showed decreased expression levels of METTL3. (C) Representative sphere images of control (shCTL) and shMETTL3 cells. (D) METTL3 KD cells showed significantly lower ability than control cells to form spheres. PCR and sphere formation assay data were analyzed by the Student's t-test and one-way ANOVA, respectively (**P<0.001, ***P<0.0001).

Statistical analysis. All data obtained were analyzed by the JMP Pro 12.2.0 software (SAS Institute, Inc., Cary, NC, USA) and described as mean ± standard error (SE). Unless stated otherwise, Student's t-test was used for statistical analysis for experimental results and the differences were considered significant.

Results

shRNA-mediated KD of METTL3. We established METTL3 KD cell lines using shRNA. Stable KD of METTL3 in RNA and protein expression was confirmed with qRT-PCR and western blot analysis, respectively (Fig. 1A and B). Although there was no difference in morphology and proliferation rate between control and METTL3 KD cells (data not shown), METTL3 KD cells in sphere formation assay showed significantly lower ability than control cells to form spheres (Fig. 1C and D).

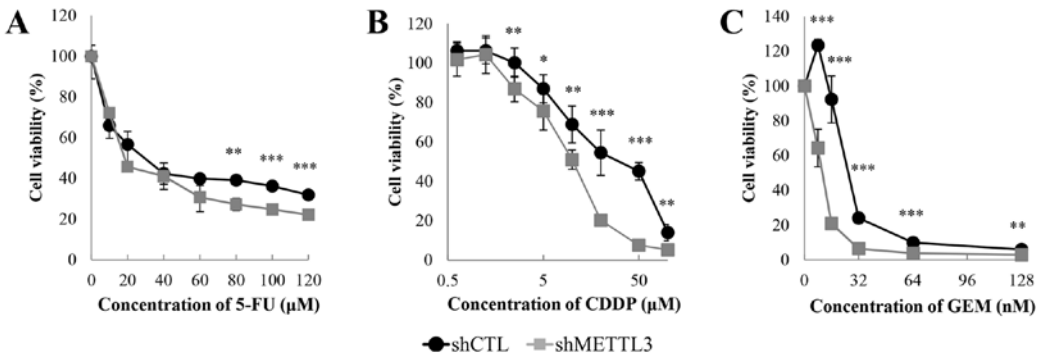

Figure 2. METTL3 depletion enhances chemosensitivity. METTL3 KD cells showed increased sensitivity to anticancer drugs: (A) 5-FU, (B) CDDP, and (C) GEM. The IC_{50} value (shCTL/shMETTL3) of each drug were as follows: 5-FU, 28.0/18.4 μM, CDDP, 33.3/10.3 μM and GEM, 25.9/10.6 nM. Data were analyzed by the Student's t-test (n=6) (*P<0.05, **P<0.01, ***P<0.001).

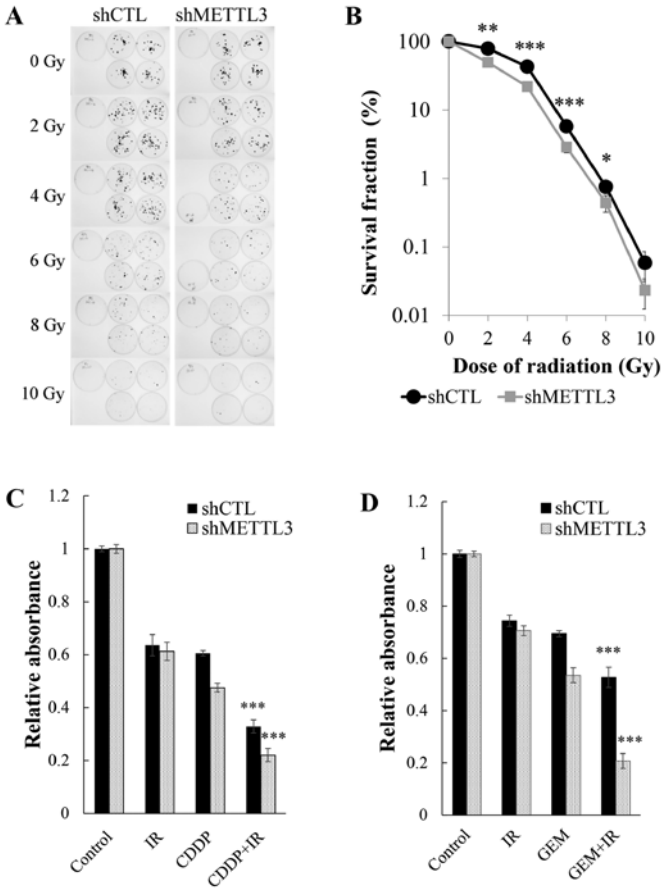

Figure 3. METTL3 depletion enhances radio- and chemoradiosensitivity. (A) Images of colonies stained by crystal violet. METTL3 KD cells showed significant susceptibility to (B) irradiation (IR) of 4 Gy as well as concurrent use of radiation and (C) CDDP or (D) GEM. Data from clonogenic assay and chemoradiosensitivity assay were analyzed by the Student's t-test (n=6) and multifactor ANOVA, respectively (*P<0.05, **P<0.01, ***P<0.001).

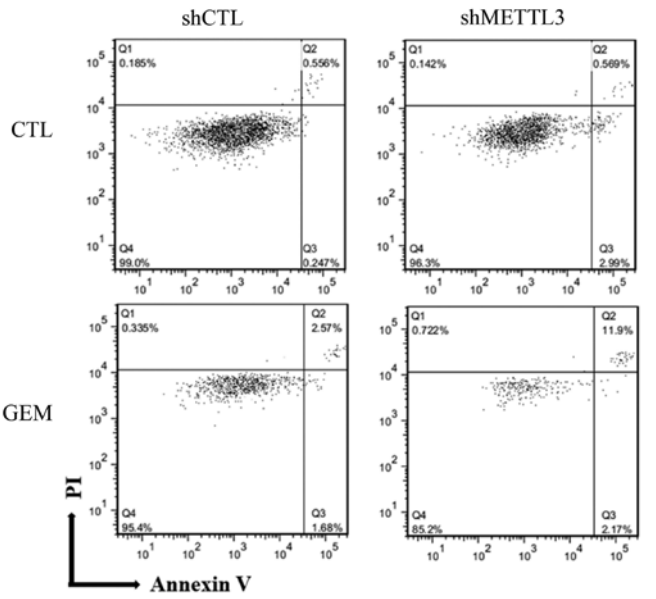

Figure 4. METTL3 depletion enhances late apoptosis in the presence of GEM. Annexin V assay in control and METTL3 KD cells. Diagrams Q1 to Q4 represent necrotic, late apoptotic, early apoptotic and live cells, respectively.

METTL3 depletion has crucial effects on chemo- and radiosensitivity. We performed crystal violet assay under administration of 5-FU, CDDP and GEM to test whether METTL3 KD alters sensitivity to anticancer agents. METTL3 depletion enhanced the sensitivity to each drug (Fig. 2). The IC_{50} values of 5-FU, CDDP and GEM were 28.0/18.4 μM (shCTL/shMETTL3), 33.3/10.3 μM and 25.9/10.6 nM, respectively. There was an obvious change in the drug sensitivity, especially in the presence of GEM. We also studied alterations of radiosensitivity derived from METTL3 KD. Clonogenic assay (Fig. 3A) revealed that METTL3 depletion resulted in enhancement of radiosensitivity with 2-8 Gy irradiation (Fig. 3B). Although no significant difference was observed with 10 Gy irradiation by statistical analysis, there was a strong tendency for shMETTL3 cells to be susceptible to irradiation, suggesting that METTL3 has important roles in the acquisition of resistance to anticancer drugs and irradiation. We next examined how toxic effects were enhanced in METTL3 KD cells when treated concurrently with drugs and irradiation at a dose of 4 Gy. The multifactor ANOVA showed a very significant effect of drug (GEM or CDDP) or radiation (P<0.0001) and significant synergistic effects of interaction (P≤0.001) in control and METTL3 KD cells (Fig. 3C and D).

Low expression of METTL3 enhances apoptotic response by GEM. The aforementioned data suggested that METTL3 is involved in apoptosis; therefore, Annexin V assay was

Table I. Top five GO terms and Reactome pathways of upregulated DEGs.

Category	Term	Count	P-value	FDR
GOTERM_BP_FAT	GO:0071357~cellular response to type I interferon	6	2.80E-05	0.0488
GOTERM_BP_FAT	GO:0060337~type I interferon signaling pathway	6	2.80E-05	0.0488
GOTERM_BP_FAT	GO:0034340~response to type I interferon	6	3.62E-05	0.0630
GOTERM_BP_FAT	GO:0032020~ISG15-protein conjugation	3	3.38E-04	0.5862
GOTERM_BP_FAT	GO:0006955~immune response	18	9.54E-04	1.647
REACTOME_PATHWAY	R-HSA-909733~Interferon α/β signaling	6	3.41E-05	0.0417
REACTOME_PATHWAY	R-HSA-168928~DDX58/IFIH1-mediated induction of interferon-α/β	3	3.99E-03	4.783
REACTOME_PATHWAY	R-HSA-936440~Negative regulators of DDX58/IFIH1 signaling	3	1.55E-02	17.417
REACTOME_PATHWAY	R-HSA-1169408~ISG15 antiviral mechanism	3	6.32E-02	55.089
REACTOME_PATHWAY	R-HSA-1236977~Endosomal/vacuolar pathway	2	6.54E-02	56.377

DEGs, differentially expressed genes; FDR, false discovery rate; GO, Gene Ontology.

Table II. Top five GO terms and Reactome pathways of downregulated DEGs.

Category	Term	Count	P-value	FDR
GOTERM_BP_FAT	GO:0043408~regulation of MAPK cascade	36	6.94.E-04	1.319
GOTERM_BP_FAT	GO:0051128~regulation of cellular component organization	93	9.23.E-04	1.749
GOTERM_BP_FAT	GO:0007010~cytoskeleton organization	52	1.38.E-03	2.602
GOTERM_BP_FAT	GO:0000226~microtubule cytoskeleton organization	25	1.63.E-03	3.065
GOTERM_BP_FAT	GO:0002821~positive regulation of adaptive immune response	9	2.01.E-03	3.769
REACTOME_PATHWAY	R-HSA-2428928~IRS-related events triggered by IGF1R	3	1.21.E-02	16.127
REACTOME_PATHWAY	R-HSA-112412~SOS-mediated signaling	3	1.67.E-02	21.4931
REACTOME_PATHWAY	R-HSA-450302~activated TAK1 mediates p38 MAPK activation	4	2.31.E-02	28.560
REACTOME_PATHWAY	R-HSA-171007~p38MAPK events	3	5.51.E-02	55.772
REACTOME_PATHWAY	R-HSA-418359~Reduction of cytosolic Ca^{++} levels	3	6.30.E-02	60.840

DEGs, differentially expressed genes; FDR, false discovery rate; GO, Gene Ontology.

conducted 48 h after treatment with GEM (Fig. 4). Compared with control cells, the percentage of late apoptotic cells was increased from 2.6 to 12% in shMETTL3 cells treated with GEM. Conversely, the percentage of live cells was decreased from 95 to 85% in shMETTL3 cells treated with GEM, suggesting that any apoptosis-related proteins were influenced by METTL3 depletion. To confirm this, we screened 35 apoptosis-related proteins using a human apoptosis proteome profiler array. No significant alteration was confirmed between shCTL and shMETTL3 cells (data not shown), implying that unknown other METTL3 target genes could be regulating apoptosis and chemo-/radiosensitivities.

Microarray data and GO analysis reveals potent target genes of METTL3. Given that METTL3 functions as m^6A writers (12,13), we are interested in the global effect on networks of mRNA expression and protein-protein interaction (PPI). A total of 735 Ensembl ID-coded differentially expressed genes were identified, of which 104 were upregulated and 631 were downregulated. To clarify the functional and pathway enrichment of differentially expressed genes, GO analysis was applied using DAVID and the top 5 GO terms and Reactome pathways of upregulated and downregulated differentially expressed genes were selected according to P-value (Tables I and II). The upregulated genes were associated primarily with immune or interferon reactions, indicating effects by shRNA transfection. Conversely, the downregulated differentially expressed genes were associated mainly with regulation of mitogen-activated protein kinase (MAPK) cascades and cellular component organization. We next focused on PPI networks of downregulated differentially expressed genes in shMETTL3 cells. The PPI analysis by STRING provided 209 nodes (genes) and 362 edges (interactions) in the network (Fig. 5), and additional MCODE analysis identified 3 modules that were associated with a ubiquitin-dependent process (including UBE2B, SOCS1, MEX3C, TRIM9, RNF25, LONRF1 and UBE2J2),

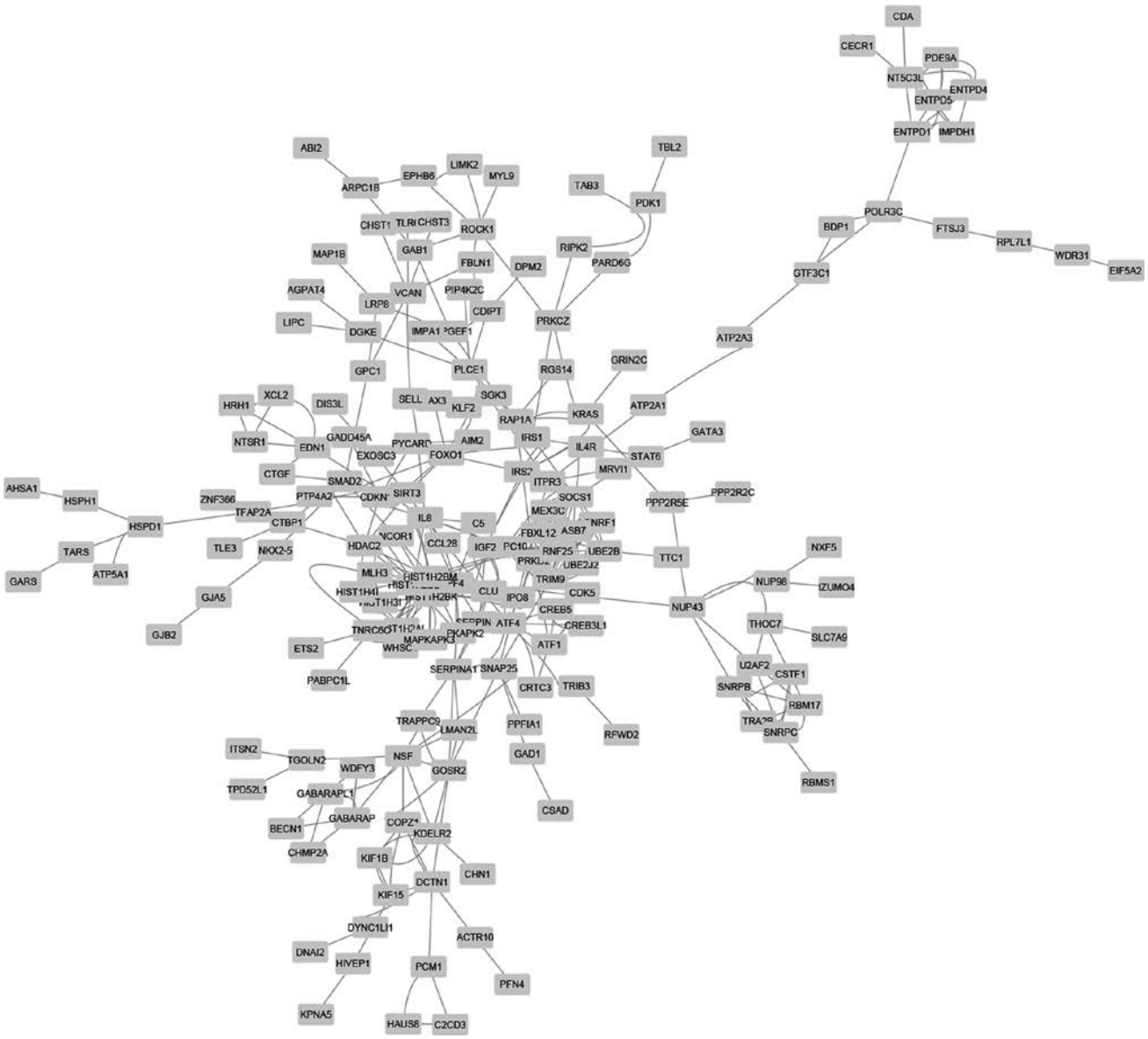

Figure 5. Predicted protein-protein interaction networks of downregulated differentially expressed genes in METTL3 KD cells. STRING database provided 209 nodes (genes) and 362 edges (interactions) in the network.

RNA splicing (including RBM17, U2AF2, SNRPC, SNRPB and CSTF1), and regulation of cellular process (including HDAC2, IGF2, MAPKAPK2 and CLU), respectively (Fig. 6 and Table III).

Discussion

In the present study, we demonstrated that METTL3 was a key protein in pancreatic cancer therapy and addressed potential targets of METTL3. METTL3 KD MIA PaCa2 cells showed lower self-renewal abilities in sphere formation assay (Fig. 1C and D) and enhanced apoptotic reactions to GEM (Fig. 4), although no significant changes were seen in morphology, proliferation rate and apoptotic reaction without drug treatment (Fig. 4). In a previous study, shRNA-mediated METTL3 KD A549 cells showed a lower proliferation rate and increased apoptosis (10). Another study showed high levels of apoptosis in small interfering RNA (siRNA)-mediated METTL3 KD HepG2 (7). For undifferentiated cells, shRNA-mediated METTL3 KD mouse embryonic stem cells (mESCs) led to a morphological change of colonies and decreased proliferation rate (17), whereas another study reported enhanced proliferation rate in CRISPR/Cas9-mediated METTL3 knockout (KO) mESCs (11). These different phenotypes could be explained by different roles of METTL3 in cell types as well as which and how many RNAs are affected by m^6A.

While investigating whether METTL3 KD affected chemo- or radiotherapy, we found that anticancer agents, 5-FU, CDDP and GEM, as well as radiation treatment significantly suppressed cell proliferation in METTL3 KD cells (Figs. 2 and 3B). Moreover, combination use of chemo- and radiotherapy led to significant synergistic effects in both cells (Fig. 3C and D). While treatment of radiation alone in chemoradiosensitivity assay was not significantly effective (Fig. 3C and D), METTL3 KD cell showed elevated sensitivity to irradiation in colony formation assay (Fig. 3B). These contrasting results could be explained by the difference of endpoints in each assay. Irradiated cells containing lethal DNA damage survived

Table III. Top three GO terms of modules in PPI of downregulated DEGs.

Category	Term	Count	P-value	FDR
Hub nodes 1				
GOTERM_BP_FAT	GO:0016567~protein ubiquitination	9	1.74E-10	2.53E-07
GOTERM_BP_FAT	GO:0032446~protein modification by small protein conjugation	9	5.40E-10	7.84E-07
GOTERM_BP_FAT	GO:0070647~protein modification by small protein conjugation or removal	9	1.81E-09	2.62E-06
Hub nodes 2				
GOTERM_BP_FAT	GO:0000377~RNA splicing, via transesterification reactions with bulged adenosine as nucleophile	5	1.02E-07	1.20E-04
GOTERM_BP_FAT	GO:0000398~mRNA splicing, via spliceosome	5	1.02E-07	1.20E-04
GOTERM_BP_FAT	GO:0000375~RNA splicing, via transesterification reactions	5	1.08E-07	1.26E-04
Hub nods 3				
GOTERM_BP_FAT	GO:0010557~positive regulation of macromolecule biosynthetic process	10	8.61E-07	1.38.E-03
GOTERM_BP_FAT	GO:0031328~positive regulation of cellular biosynthetic process	10	1.70E-06	2.72.E-03
GOTERM_BP_FAT	GO:0009891~positive regulation of biosynthetic process	10	1.97E-06	3.16.E-03

DEGs, differentially expressed genes; FDR, false discovery rate; GO, Gene Ontology.

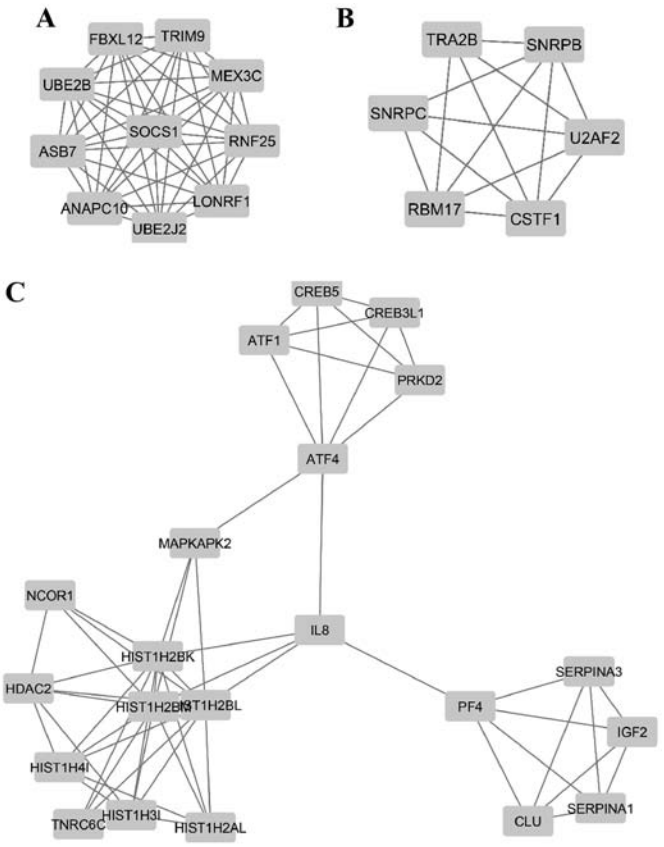

Figure 6. Three highly interconnected regions were detected as modules in the PPI network of downregulated differentially expressed genes in METTL3 KD cells. Genes in (A) module 1, (B) module 2 and (C) module 3 were associated with ubiquitin-dependent process, RNA splicing and regulation of the cellular process, respectively.

only a short time; however, they were unable to form colonies for a few weeks. A recent study revealed that m^{6}A was induced rapidly at the sites of DNA damage after ultraviolet irradiation (UVC), and METTL3 KO cells showed delayed repair of UVC-induced DNA damage and higher sensitivity to UVC compared to controls (26), suggesting the importance of METTL3 in the recovery from UVC-induced DNA damage. It is interesting to note that, in that study, γ-irradiation did not induce m^{6}A within 1 min. Therefore, our results provided the possibility of another unknown mechanism by which METTL3 regulates radiation-induced DNA damage. Today, GEM- and 5-FU-based chemotherapy as well as concurrent chemoradiation therapy are key treatments in advanced pancreatic cancer (33). Taken together, our findings indicate that METTL3 is a potent target for pancreatic cancer treatment.

From cDNA microarray data, several processes and cascades emerged as potential targets of METTL3: MAPK cascades, ubiquitin-dependent process, RNA splicing and regulation of the cellular process (Fig. 6 and Tables II and III). MAPK cascades are involved in various essential cellular processes such as proliferation, differentiation, stress response, DNA repair, apoptosis and survival (34,35). Histone deacetylase 2 (HDAC2) plays a crucial role in DNA double-strand break repair and cancer malignancy (36,37). Insulin-like growth factor 2 (IGF-2) and IGF signaling are important for cancer development and progression (38). MAP kinase-activated protein kinase 2 (MAPKAPK2), a member of the Ser/Thr protein kinase family, is shown to participate in inflammatory response, gene transcription, and cell cycle regulation (39,40). Clusterin (CLU) is a key protein in stress response and cell survival. Accumulating data revealed that CLU is associated with resistance to chemotherapy and radiotherapy, through various pathways including inhibition of BAX (bcl-2-like protein 4), activation of ERK1/2 and phosphoinositide 3-kinase (PI3K)-Akt signaling pathway (41,42). Collectively, our finding raises the possibility that METTL3 modulates MAPK cascade and cellular processes, resulting in resistance to chemo- and radiotherapy.

This study also showed that ubiquitin-dependent process is a possible target of METTL3 (Fig. 6A and Table III). Ubiquitination requires 3 steps, activation, conjugation, and ligation, and is performed using ubiquitin-activating enzymes (E1s), ubiquitin-conjugating enzymes (E2s) and ubiquitin ligases (E3s), respectively. According to recent reports, these proteins play an important role in cancer malignancy. Ubiquitin-conjugating enzyme E2B (UBE2B, also called Rad6B), which works as a DNA repair protein, is associated with chemoresistance and cell stemness in ovarian cancer cells (43). Suppressor of cytokine signaling 1 (SOCS1) is generally known to provide a negative feedback of cytokine signaling though the JAK/STAT3 pathway and suppress insulin signaling by ubiquitin-mediated degradation of insulin receptor substrate (IRS) (44). Notably, SOCS1 is reported as an oncogene and a tumor suppressor in cancer (45). Mex-3 RNA-binding family member C (MEX-3C), a family of RNA-binding E3 ubiquitin-protein ligase, is suggested to be involved in mRNA decay (46). Recently, MEX-3C was suggested as a new chromosomal instability (CIN) suppressor in CIN^+ colorectal cancer (47), possibly contributing to chromosome segregation errors and DNA damage. Taken together, our data indicate that METTL3 alters ubiquitination-related protein expression, leading to genomic instability and insufficient DNA damage repair.

Furthermore, we found that the RNA splicing process was a potent target process of METTL3 (Fig. 6B and Table III). Alternative pre-mRNA splicing in which intronic sequences are removed stepwise is an essential process in producing encoded proteins. Aberrations of splicing by altered spliceosome proteins lead to gain-, loss- and opposite-of-function mutations, contributing to alteration of tumor characteristics (48,49). A recent report suggested that splicing factor U2AF 65 kDa subunit (U2AF2) is required for efficient DNA repair (50). In addition, while its mechanism is still unknown, RNA-binding motif protein 17 (RBM17, also called SPF45) induces resistance to various anticancer drugs (51). Small nuclear ribonucleoprotein-associated proteins B and B' (SNRPB) are suggested to be involved in RNA processing and DNA repair in glioblastoma (52). Notably, SNRPB is associated with crucial genes including RTK, PI3K, MAPK, RAS, AKT, RB and p53, which are involved in essential cellular processes (52). Collectively, our findings indicate that METTL3 alters splicing regulator expression, resulting in unexpected splicing events including insufficient DNA repair.

We note several limitations to this study. First, our *in vitro* experiments and results are based on a single cell line; however, additional confirming studies are necessary in other cell lines. Second, possible targets of METTL3 are derived from microarray data mining. Currently, microarray technology is a powerful tool to screen gene-expression profiling. However, actual protein expression levels are not confirmed. In addition, genes with a <2-fold change in expression are excluded from GO analysis and PPI analysis, which may lead to inaccurate conclusions.

In summary, the present study demonstrates that METTL3 is associated with therapeutic resistance and is a potential therapeutic target of pancreatic cancer. Additionally, our findings suggest several critical pathways, including MAPK cascades, ubiquitin-dependent process, RNA splicing and regulation of cellular process, as possible targets of METTL3. Alteration of these processes triggers various aberrant biological behaviors that could lead to cancer progression and therapeutic resistance. Further studies on the interactions between METTL3 and these processes are critical for understanding the functional mechanisms of METTL3.

Acknowledgements

The authors thank our laboratory members for fruitful discussions, N. Nishida, K. Otani and K. Tamari for helpful suggestions, and M. Ozaki and Y. Noguchi for excellent technical support. Flow cytometric analysis was performed with equipment in the Center for Medical Research and Education, Graduate School of Medicine, Osaka University, Japan. This study received financial support from grants-in-aid for Scientific Research and P-DIRECT and P-CREATE Grants from the Ministry of Education, Culture, Sports, Science, and Technology, MEXT (MK, YD, MM, HI, and KO); Kobayashi Foundation for Cancer Research (HI); Kobayashi International Scholarship Foundation (MK, HI); and a grant-in-aid from the Ministry of Health, Labor, and Welfare (MK, YD, MM, HI, and KO). Institutional endowments were received from Taiho Pharmaceutical Co., Ltd. (Tokyo, Japan), Evidence Based Medical Research Center INC. (Osaka, Japan), UNITECH Co., Ltd. (Chiba, Japan), IDEA Consultants, Inc. (Tokyo, Japan), and Kinshu-kai Medical Corporation (Osaka, Japan). These funders had no role in the main experimental equipment, supply expenses, study design, data collection and analysis, decision to publish, or preparation of the present study.

References

1. Waddington CH: The epigenotype. Endeavour 1: 18-20, 1942.
2. Cantara WA, Crain PF, Rozenski J, McCloskey JA, Harris KA, Zhang X, Vendeix FA, Fabris D and Agris PF: The RNA Modification Database, RNAMDB: 2011 update. Nucleic Acids Res 39 (Database): D195-D201, 2011.
3. Ping XL, Sun BF, Wang L, Xiao W, Yang X, Wang WJ, Adhikari S, Shi Y, Lv Y, Chen YS, *et al*: Mammalian WTAP is a regulatory subunit of the RNA N6-methyladenosine methyltransferase. Cell Res 24: 177-189, 2014.
4. Liu J, Yue Y, Han D, Wang X, Fu Y, Zhang L, Jia G, Yu M, Lu Z, Deng X, *et al*: A METTL3-METTL14 complex mediates mammalian nuclear RNA N6-adenosine methylation. Nat Chem Biol 10: 93-95, 2014.
5. Perry RP and Kelley DE: Existence of methylated messenger RNA in mouse L cells. Cell 1: 37-42, 1974.
6. Desrosiers R, Friderici K and Rottman F: Identification of methylated nucleosides in messenger RNA from Novikoff hepatoma cells. Proc Natl Acad Sci USA 71: 3971-3975, 1974.
7. Dominissini D, Moshitch-Moshkovitz S, Schwartz S, Salmon-Divon M, Ungar L, Osenberg S, Cesarkas K, Jacob-Hirsch J, Amariglio N, Kupiec M, *et al*: Topology of the human and mouse m^6A RNA methylomes revealed by m^6A-seq. Nature 485: 201-206, 2012.
8. Meyer KD, Saletore Y, Zumbo P, Elemento O, Mason CE and Jaffrey SR: Comprehensive analysis of mRNA methylation reveals enrichment in 3' UTRs and near stop codons. Cell 149: 1635-1646, 2012.
9. Wang X, Lu Z, Gomez A, Hon GC, Yue Y, Han D, Fu Y, Parisien M, Dai Q, Jia G, *et al*: N^6-methyladenosine-dependent regulation of messenger RNA stability. Nature 505: 117-120, 2014.
10. Lin S, Choe J, Du P, Triboulet R and Gregory RI: The m^6A Methyltransferase METTL3 promotes translation in human cancer cells. Mol Cell 62: 335-345, 2016.

11. Batista PJ, Molinie B, Wang J, Qu K, Zhang J, Li L, Bouley DM, Lujan E, Haddad B, Daneshvar K, *et al*: m^{6}A RNA modification controls cell fate transition in mammalian embryonic stem cells. Cell Stem Cell 15: 707-719, 2014.
12. Jia G, Fu Y, Zhao X, Dai Q, Zheng G, Yang Y, Yi C, Lindahl T, Pan T, Yang YG, *et al*: *N*^{6}-methyladenosine in nuclear RNA is a major substrate of the obesity-associated FTO. Nat Chem Biol 7: 885-887, 2011.
13. Zheng G, Dahl JA, Niu Y, Fedorcsak P, Huang CM, Li CJ, Vågbø CB, Shi Y, Wang WL, Song SH, *et al*: ALKBH5 is a mammalian RNA demethylase that impacts RNA metabolism and mouse fertility. Mol Cell 49: 18-29, 2013.
14. Liu N, Dai Q, Zheng G, He C, Parisien M and Pan T: *N*^{6}-methyladenosine-dependent RNA structural switches regulate RNA-protein interactions. Nature 518: 560-564, 2015.
15. Fustin JM, Doi M, Yamaguchi Y, Hida H, Nishimura S, Yoshida M, Isagawa T, Morioka MS, Kakeya H, Manabe I, *et al*: RNA-methylation-dependent RNA processing controls the speed of the circadian clock. Cell 155: 793-806, 2013.
16. Du H, Zhao Y, He J, Zhang Y, Xi H, Liu M, Ma J and Wu L: YTHDF2 destabilizes m^{6}A-containing RNA through direct recruitment of the CCR4-NOT deadenylase complex. Nat Commun 7: 12626, 2016.
17. Wang Y, Li Y, Toth JI, Petroski MD, Zhang Z and Zhao JC: *N*^{6}-methyladenosine modification destabilizes developmental regulators in embryonic stem cells. Nat Cell Biol 16: 191-198, 2014.
18. Meyer KD, Patil DP, Zhou J, Zinoviev A, Skabkin MA, Elemento O, Pestova TV, Qian SB and Jaffrey SR: 5' UTR m^{6}A promotes cap-independent translation. Cell 163: 999-1010, 2015.
19. Zhou J, Wan J, Gao X, Zhang X, Jaffrey SR and Qian SB: Dynamic m^{6}A mRNA methylation directs translational control of heat shock response. Nature 526: 591-594, 2015.
20. Xiao W, Adhikari S, Dahal U, Chen YS, Hao YJ, Sun BF, Sun HY, Li A, Ping XL, Lai WY, *et al*: Nuclear m^{6}A reader YTHDC1 regulates mRNA splicing. Mol Cell 61: 507-519, 2016.
21. Alarcón CR, Lee H, Goodarzi H, Halberg N and Tavazoie SF: *N*^{6}-methyladenosine marks primary microRNAs for processing. Nature 519: 482-485, 2015.
22. Alarcón CR, Goodarzi H, Lee H, Liu X, Tavazoie S and Tavazoie SF: HNRNPA2B1 is a mediator of m^{6}A-dependent nuclear RNA processing events. Cell 162: 1299-1308, 2015.
23. Chen T, Hao YJ, Zhang Y, Li MM, Wang M, Han W, Wu Y, Lv Y, Hao J, Wang L, *et al*: m^{6}A RNA methylation is regulated by microRNAs and promotes reprogramming to pluripotency. Cell Stem Cell 16: 289-301, 2015.
24. Geula S, Moshitch-Moshkovitz S, Dominissini D, Mansour AA, Kol N, Salmon-Divon M, Hershkovitz V, Peer E, Mor N, Manor YS, *et al*: Stem cells. m^{6}A mRNA methylation facilitates resolution of naïve pluripotency toward differentiation. Science 347: 1002-1006, 2015.
25. Patil DP, Chen CK, Pickering BF, Chow A, Jackson C, Guttman M and Jaffrey SR: m^{6}A RNA methylation promotes XIST-mediated transcriptional repression. Nature 537: 369-373, 2016.
26. Xiang Y, Laurent B, Hsu CH, Nachtergaele S, Lu Z, Sheng W, Xu C, Chen H, Ouyang J, Wang S, *et al*: RNA m^{6}A methylation regulates the ultraviolet-induced DNA damage response. Nature 543: 573-576, 2017.
27. Zhang SY, Zhang SW, Liu L, Meng J and Huang Y: m^{6}A-Driver: Identifying context-specific mRNA m^{6}A methylation-driven gene interaction networks. PLOS Comput Biol 12: e1005287, 2016.
28. Franken NA, Rodermond HM, Stap J, Haveman J and van Bree C: Clonogenic assay of cells in vitro. Nat Protoc 1: 2315-2319, 2006.
29. Huang W, Sherman BT and Lempicki RA: Systematic and integrative analysis of large gene lists using DAVID bioinformatics resources. Nat Protoc 4: 44-57, 2009.
30. Szklarczyk D, Morris JH, Cook H, Kuhn M, Wyder S, Simonovic M, Santos A, Doncheva NT, Roth A, Bork P, *et al*: The STRING database in 2017: Quality-controlled protein-protein association networks, made broadly accessible. Nucleic Acids Res 45 (D1): D362-D368, 2017.
31. Shannon P, Markiel A, Ozier O, Baliga NS, Wang JT, Ramage D, Amin N, Schwikowski B and Ideker T: Cytoscape: A software environment for integrated models of biomolecular interaction networks. Genome Res 13: 2498-2504, 2003.
32. Bader GD and Hogue CW: An automated method for finding molecular complexes in large protein interaction networks. BMC Bioinformatics 4: 2, 2003.
33. Tempero MA, Malafa MP, Al-Hawary M, Asbun H, Bain A, Behrman SW, Benson AB III, Binder E, Cardin DB, Cha C, *et al*: Pancreatic adenocarcinoma, version 2.2017, NCCN Clinical Practice Guidelines in Oncology. J Natl Compr Cancer Netw 15: 1028-1061, 2017.
34. Dhillon AS, Hagan S, Rath O and Kolch W: MAP kinase signalling pathways in cancer. Oncogene 26: 3279-3290, 2007.
35. Corre I, Paris F and Huot J: The p38 pathway, a major pleiotropic cascade that transduces stress and metastatic signals in endothelial cells. Oncotarget 8: 55684-55714, 2017.
36. Gong F and Miller KM: Mammalian DNA repair: HATs and HDACs make their mark through histone acetylation. Mutat Res 750: 23-30, 2013.
37. Shan W, Jiang Y, Yu H, Huang Q, Liu L, Guo X, Li L, Mi Q, Zhang K and Yang Z: HDAC2 overexpression correlates with aggressive clinicopathological features and DNA-damage response pathway of breast cancer. Am J Cancer Res 7: 1213-1226, 2017.
38. Livingstone C: IGF2 and cancer. Endocr Relat Cancer 20: R321-R339, 2013.
39. Cargnello M and Roux PP: Activation and function of the MAPKs and their substrates, the MAPK-activated protein kinases. Microbiol Mol Biol Rev 75: 50-83, 2011.
40. Moens U, Kostenko S and Sveinbjørnsson B: The role of mitogen-activated protein kinase-activated protein kinases (MAPKAPKs) in inflammation. Genes (Basel) 4: 101-133, 2013.
41. Koltai T: Clusterin: A key player in cancer chemoresistance and its inhibition. Onco Targets Ther 7: 447-456, 2014.
42. Albany C and Hahn NM: Heat shock and other apoptosis-related proteins as therapeutic targets in prostate cancer. Asian J Androl 16: 359-363, 2014.
43. Somasagara RR, Spencer SM, Tripathi K, Clark DW, Mani C, Madeira da Silva L, Scalici J, Kothayer H, Westwell AD, Rocconi RP, *et al*: RAD6 promotes DNA repair and stem cell signaling in ovarian cancer and is a promising therapeutic target to prevent and treat acquired chemoresistance. Oncogene: Aug 14, 2017 (Epub ahead of print). doi: 10.1038/onc.2017.279.
44. Rui L, Yuan M, Frantz D, Shoelson S and White MF: SOCS-1 and SOCS-3 block insulin signaling by ubiquitin-mediated degradation of IRS1 and IRS2. J Biol Chem 277: 42394-42398, 2002.
45. Beaurivage C, Champagne A, Tobelaim WS, Pomerleau V, Menendez A and Saucier C: SOCS1 in cancer: An oncogene and a tumor suppressor. Cytokine 82: 87-94, 2016.
46. Cano F, Rapiteanu R, Sebastiaan Winkler G and Lehner PJ: A non-proteolytic role for ubiquitin in deadenylation of MHC-I mRNA by the RNA-binding E3-ligase MEX-3C. Nat Commun 6: 8670, 2015.
47. Burrell RA, McClelland SE, Endesfelder D, Groth P, Weller MC, Shaikh N, Domingo E, Kanu N, Dewhurst SM, Gronroos E, *et al*: Replication stress links structural and numerical cancer chromosomal instability. Nature 494: 492-496, 2013.
48. Eblen ST: Regulation of chemoresistance via alternative messenger RNA splicing. Biochem Pharmacol 83: 1063-1072, 2012.
49. Zhang J and Manley JL: Misregulation of pre-mRNA alternative splicing in cancer. Cancer Discov 3: 1228-1237, 2013.
50. Savage KI, Gorski JJ, Barros EM, Irwin GW, Manti L, Powell AJ, Pellagatti A, Lukashchuk N, McCance DJ, McCluggage WG, *et al*: Identification of a BRCA1-mRNA splicing complex required for efficient DNA repair and maintenance of genomic stability. Mol Cell 54: 445-459, 2014.
51. Perry WL III, Shepard RL, Sampath J, Yaden B, Chin WW, Iversen PW, Jin S, Lesoon A, O'Brien KA, Peek VL, *et al*: Human splicing factor SPF45 (RBM17) confers broad multidrug resistance to anticancer drugs when overexpressed - a phenotype partially reversed by selective estrogen receptor modulators. Cancer Res 65: 6593-6600, 2005.
52. Correa BR, de Araujo PR, Qiao M, Burns SC, Chen C, Schlegel R, Agarwal S, Galante PA and Penalva LO: Functional genomics analyses of RNA-binding proteins reveal the splicing regulator SNRPB as an oncogenic candidate in glioblastoma. Genome Biol 17: 125, 2016.